

Numerical simulation of a soft-x-ray Li laser pumped with synchrotron radiation

Balazs Rozsnyai

Lawrence Livermore National Laboratory, University of California, Livermore, California 94550

Hiroshi Watanabe and Paul L. Csonka*

Institute of Theoretical Science, University of Oregon, Eugene, Oregon 97403

(Received 20 February 1985)

Results of a computer simulation are reported for a lithium soft-x-ray laser pumped by synchrotron radiation. Coherent stimulated emission of the photons of interest occurs in $\text{Li II } 1s2p \rightarrow \text{Li II } 1s^2$ transitions. Calculated results include the dominant ion and photon densities and the laser gain.

I. INTRODUCTION

A. Background

It was suggested some time ago that coherent x rays could be produced by pumping an appropriate material with synchrotron radiation.^{1,2} In particular, it was pointed out that a soft-x-ray laser operating at wavelength $\lambda = 199.3 \text{ \AA}$ could be constructed by pumping a Li gas with synchrotron-radiation photons of energy $E_x > 66.3 \text{ eV}$. In this paper we report the results of a computer simulation carried out to evaluate the capabilities of such a Li x-ray laser.

The literature contains several interesting descriptions for other proposed Li soft-x-ray laser construction schemes.^{3,4} The reader may wonder why, in view of those, we choose to continue pursuing our originally suggested approach. It is, therefore, appropriate—indeed it is expected of us—to point out the advantages of our method. Before doing that, however, we wish to emphasize that it is not our aim here to dispute the relative merit of the various alternative methods of x-ray laser construction. Instead, we believe that a variety of approaches to this new and exciting subject is desirable. Some approaches will undoubtedly turn out to be more appropriate for certain applications than others and, in any case, progress achieved in one will facilitate progress in others. Having said that, we now list those general features of synchrotron radiation (SR) which are advantageous for x-ray laser pumping.

B. Characteristics of synchrotron radiation (SR) favorable for coherent photon generation

(1) SR is emitted from high-energy storage rings in short bursts. The pulse length is usually $\tau \leq 10^2 \text{ ps}$, and $\tau \leq 10 \text{ ps}$ will be produced by the next generation of rings. Since x-ray lasers are energy intensive, and excited ionic states tend to decay quickly, high instantaneous pumping intensity is advantageous. (The often annoying problem of excessive plasma preheating can thus also be reduced.)

(2) The radiation can be focused on a small area, $A < 10^{-6} \text{ cm}^2$. Therefore, the energy density delivered

per unit surface can be higher than for many other sources.

(3) SR is emitted with a small angular divergence, typically $\Delta\theta \leq 1 \text{ mrad}$. Therefore, the phase-space density of photons is high. This feature allows one to choose a variety of pumping schemes (e.g., longitudinal: along the length of the lasing medium, or transverse: across it, or oblique: intermediate between these two).

(4) The energy spectrum of SR can be readily tailored to the requirements of laser pumping. High quality optical elements, such as monochromators, mirrors, filters, etc., have been developed and are routinely available for this purpose. That enables one to eliminate unwanted frequencies—a task difficult and even impossible to achieve in certain other schemes of x-ray laser construction.

(5) SR can be accommodated to a wide variety of geometries: one is not restricted to “cramped” geometrical configurations. For example, since SR has low angular divergence, the lasing material need not be located near the source of radiation, nor close to any of the optical elements.

(6) SR energy can be selectively deposited into those places where it is wanted. Only a relatively small fraction of the energy need be deposited into unwanted states. In the particular case we propose to realize, this fraction can be $< 10\%$. By contrast, in processes where a flashlamp is used for pumping, for example, an overwhelming fraction of the energy is expended to heat the flashlamp material. While this is no drawback in situations where ample energy is available, in more common circumstances energy efficiency is a desirable attribute.

(7) Since SR can be well focused, lasing can take place in a small volume (typically $< 1 \text{ cm} \times 100 \text{ }\mu\text{m}^2$). As a result, it is easy to get radiation into and out of the volume, absorption can be kept at a manageable level.

(8) Since the pumping energy is deposited selectively, the plasma of lasing ions can be kept relatively cool. That, in turn, implies reduced homogeneous and reduced inhomogeneous line broadening, both of which result in an enhanced laser gain.

(9) A typical high-energy electron storage ring pro-

duces bursts of SR with a repetition rate of $\geq 10^6$ Hz. Consequently, even in cases when the total number of coherent photons produced by a single SR burst may be small, the potential time-averaged power density delivered by such a device can be impressive.

C. Recent advances in instrumentation and techniques

During the last several years, experimentation with SR has reached a new level of sophistication. Many developments which were foreseen^{1,2} at the time when x-ray laser pumping with SR was first suggested, have since been realized. High-energy electron storage-ring operation dedicated to SR research has become routine. Work is continuing on a progressive reduction of photon emittances generated by electron storage rings.⁵ Wigglers and undulators have been installed in several rings,⁶ and our understanding of their operation has become more complete,^{7,8} resulting in an increase of produced photon brightness. Improved x-ray mirrors^{9,10} and gratings^{11,12} have become available, and further improvements in the performance and understanding of x-ray gratings,^{13,14} zone plates,¹⁵ and monochromators are within reach. Furthermore, the radiated intensity of soft-x-ray photons could be increased by at least two additional orders of magnitude, by microbunching the electron beam which circulates in the storage ring.^{16,17} Even without this last development, however, enough radiated photon brilliance can be generated to achieve x-ray laser operation. Thus the field has now reached the necessary maturity to support rapid progress toward a SR pumped x-ray laser.

In anticipation of the developments just reviewed, calculations were carried out over the last several years to evaluate the potential of synchrotron-radiation pumping for coherent x-ray generation. While preliminary calculations covered some heavier elements as well,¹⁸ computer simulations performed at the Lawrence Livermore National Laboratory and at the University of Oregon concentrated on studying soft coherent x-ray production from a Li plasma. The results of these calculations are encouraging enough to warrant their publication at this time.

II. COHERENT PHOTON GENERATION

The relevant energy levels of Li I and Li II are shown in Fig. 1. Lasing could be induced between several level pairs. Here we report the results of calculations evaluating the characteristics of lasing transitions between the states Li II $1s2p$ and Li II $1s^2$. Figure 2 illustrates the process: At first, neutral Li (denoted as Li I) is ionized by SR photons whose energy, E_x , must exceed the Li I K edge located at 66.3 eV. Next, the resulting once-ionized Li (denoted as Li II) is irradiated by infrared photons of energy $E_\Delta = 1.2965$ eV. We will refer to these photons as "low-energy radiation." This radiation will cause transitions Li II $1s2s \rightleftharpoons$ Li II $1s2p$ so that at saturation the number of Li II $1s2s$ ions equals that of the Li II $1s2p$ ions whose radiative lifetime is $\tau_R = 3.9 \times 10^{-11}$ sec. Finally the Li II $1s2p$ ions are coherently deexcited via stimulated emission by photons of energy $E_l = 62.2$ eV into the

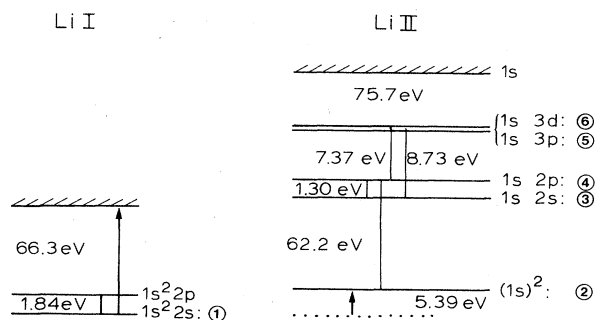


FIG. 1. Li I and Li II energy levels.

ground state of the lasing transition: Li II $1s^2$. During this process a burst of coherent photons will be produced, each with energy E_l . This laser action is a "self-terminating" one, i.e., the inversion lasts only as long as the lifetime of the upper state. In our case, however, that is no drawback, because the pumping SR energy can be delivered fast enough.

Instead of irradiating Li II ions with $E_\Delta = 1.2965$ eV radiation, one can, essentially equivalently, irradiate Li I atoms by photons with energy $E_\Delta = 1.84$ eV, which will induce Li I $1s^2 2s \rightleftharpoons$ Li I $1s^2 2p$ transitions. At saturation these photons would cause the number of Li I $1s^2 2p$ atoms to approach that of the Li I $1s^2 2s$ atoms. Furthermore, if the electron density in the lasing medium is high enough, then electron impact alone will be able to generate the necessary number of Li II $1s2p$ ions; in that case no low photons with energy E_Δ would be needed. On the other hand, electron impact will also produce undesirable transitions which limits the permissible electron density within the lasing volume.

The lasing medium is to be contained in a volume as shown in Fig. 3, a cylinder of length d_z , whose normal cross section is an ellipse with major diameter d_x and minor diameter d_y . The dimensions of the volume are to be matched to the parameters of the pumping SR generated by an electron storage ring such as SPEAR. These parameters will be determined by the storage-ring emittance, the SR intensity, and the density of the lasing medium. The contemplated dimensions of the lasing

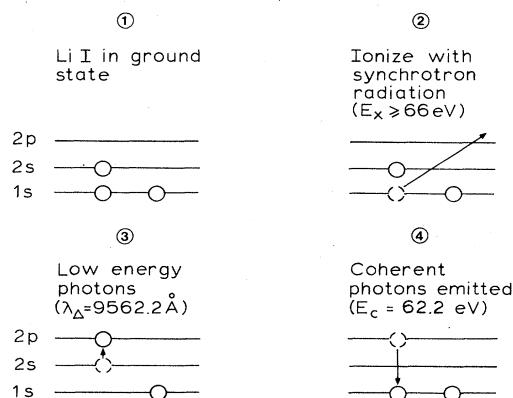


FIG. 2. Generation of coherent photons in lithium.

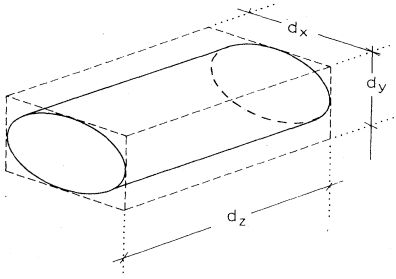


FIG. 3. The volume which contains the lasing medium.

volume are $d_x, d_y \leq 100 \mu\text{m}$, and d_z of the order of 1 cm. Clearly, one expects to encounter no difficulty getting the low-energy photons to traverse such a volume.

The method of irradiating the lasing volume will depend on the chosen SR source. One can illuminate the volume longitudinally or transversely (i.e., parallel to the side d_z in Fig. 3, or perpendicularly to it), or choose the illuminating beam axis at an angle ϕ with respect to the volume axis. For longitudinal illumination, it is useful to estimate the number N_x of SR photons needed for efficient x-ray operation (i.e., when the number of coherent photons is comparable to the number of absorbed SR photons) from the formula²

$$N_x \geq 8\epsilon_x^{1/2}\epsilon_y^{1/2}g^{-2}N_4^{-1}\sigma_s^{-2} \times \left[\ln \left(\frac{4\epsilon_x^{1/2}\epsilon_y^{1/2}d_z}{\sigma_s} \right) \right]^2 \epsilon_\gamma^{-1}, \quad (1a)$$

where ϵ_x and ϵ_y are the horizontal and vertical emittances of the synchrotron radiation beam; σ_s is the cross section for stimulated $\text{Li}^+(1s2p)\text{-Li}^+(1s^2)$ transitions; ϵ_γ is the average fraction of synchrotron-radiation photons absorbed by the sample; $g \leq 1$ is the fraction of $\text{Li}^+(1s2p)$ ions which satisfy both of the following conditions: the two electrons are in a singlet spin state ($S=0$), and, also, the orbital angular momentum of the $2p$ electron is parallel to the spin of the photons produced in the lasing transitions; N_4 is the density of $\text{Li}^+(1s2p)$ ions. For transverse illumination the requirements

$$d_z < c\tau$$

and

$$N_x > 2^{1/2} \times 4\epsilon_y^{1/2}(\sigma_s\sigma_{pa}gN_1)^{-1}d_x^{1/2} \ln \left(\frac{2\epsilon_y^{1/2}d_x^{3/2}}{\sigma_s} \right) \quad (1b)$$

are approximate limiting conditions, where $\tau \leq \tau_R$ is the lifetime of the $\text{Li II } 1s2p$ ionic species, σ_{pa} is the cross section for removing a $1s$ electron from $\text{Li I } 1s^22s$, and N_1 is the number density of $\text{Li I } 1s^22s$ atoms. More exact results are furnished by the computer results, as reported below.

It is anticipated that the pumping x-ray photons will be generated by an electron beam passing through either a wiggler magnet or an appropriately tuned undulator located in a storage ring, such as SPEAR at Stanford. If the

first-order energy peak of the undulator is chosen to be near the $\text{Li I } K$ edge of energy $E_{x,K}=66.3$ eV, then the undulator source itself will effectively serve as a partial radiation filter, producing most photons with energies typically within 10% of $E_{x,K}$. In any case, proper monochromatization will ensure that only pumping photons with energy E_x within the interval $E_{x,L} \leq E_x \leq E_{x,M}$ are admitted to the lasing medium, where $E_{x,K} \leq E_{x,L}$.

As the generated pumping radiation beam leaves the port which serves as the radiation source, and enters the experimental area, it has to be focused onto the lasing volume. Focusing can be achieved either by mirrors or by diffractive elements such as zone plates. Details of the focusing will depend on the chosen parameters of target illumination, including the relative direction of the pumping beam and the axis of the lasing volume. Those parameters can be selected (e.g., by the computer program) once the properties of the pumping radiation and those of the lasing medium have been fixed.

To prevent premature triggering of induced ionic deexcitations of the type $\text{Li II } 1s2p \rightarrow \text{Li II } 1s^2$, one has to ensure that the flux of photons with energy E_l traveling from the port of the lasing medium, is sufficiently low. That can be achieved by interposing an appropriate ion filter¹⁹ which will preferentially deplete the number of unwanted photons.

For the particular soft-x-ray laser under discussion here, it is desirable to reduce the risetime, τ_{SR} of the SR pumping pulse to values $\tau_{\text{SR}} \leq 3 \times 10^{-12}$ sec, to limit plasma preheating. That, in turn, will increase the efficiency of coherent photon generation because, first it reduces the fraction of energy diverted into the production of unneeded states, and second, it also suppresses the appearance of undesirable states which would tend to inhibit coherent photon generation. The desired risetimes can be reached by means of an appropriate shielding²⁰ interposed between the SR port and the lasing medium.

If the low-energy photon energy is chosen to be $E_\Delta=1.2965$ eV, then the low-energy photon beam has to be switched on essentially simultaneously with the pumping SR pulse. On the other hand, if $E_\Delta=1.84$ eV is chosen, then the low-energy photon flux is to be turned on sufficiently in advance of the pumping SR pulse, that the density of $\text{Li I } 1s^22p$ atoms will approximately equal the $\text{Li I } 1s^22s$ atom density by the time the SR pulse reaches the lasing volume. In any case, the low-energy photons may traverse the lasing volume along the minor axis of its cross-sectional ellipse.

The pulse of coherent photons of energy E_l will propagate lengthwise along the axis of the target. Thus it has a distinctive signature in space as well as energy, which facilitates detection.

The results of calculations reported later in this paper show that with present-day electron storage rings each SR pulse can have enough pumping photons to generate a coherent photon pulse per SR pulse. However, during the process of generation, the lasing medium is ionized, heated, and otherwise modified so that it may not be suitable to serve again as the lasing medium for some time after a coherent pulse has been generated. On the other hand, presently operating electron storage rings are capable of

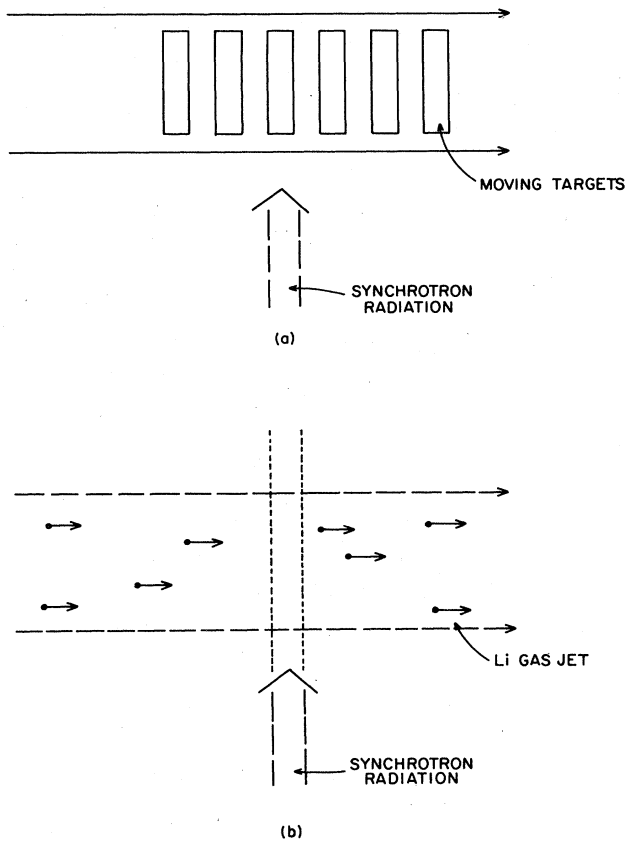


FIG. 4. (a) A sequence of solid Li targets are printed on a moving ribbon. Successive bursts of coherent photons are generated in successive Li targets placed in the path of the SR beam. (b) A jet of Li atoms passes through the SR beam. New atoms move into the beam prior to each burst of coherent photons generated in the Li-jet gas target.

producing of the order of 10^6 – 10^8 SR pulses per second. It would be desirable to be able to harness all of them for purposes of coherent photon generation. Figures 4(a) and 4(b) illustrate two arrangements which will make this possible. Figure 4(a) shows blocks of solid Li imprinted on a ribbon which is then moved across the photon beams, thus replacing one used target with a fresh one after each SR pulse. This method is adequate, if the frequency of SR pulses does not exceed $\nu_{\text{SR}} \approx 10^6 \text{ sec}^{-1}$. In Fig. 4(b) a jet of Li atoms streams across the pumping photon beam. The gas volume illuminated by each SR pulse serves as the lasing volume for that pulse. This method may be used up to $\nu_{\text{SR}} \approx 10^8 \text{ sec}^{-1}$.

III. COMPUTER SIMULATION

A. General characteristics

We constructed a computer program to simulate the time evolution of the lasing medium during and after SR pumping. The program gives the time history of all important ionic densities, the neutral atom density, free electronic density, the densities of all photons which can be produced in transitions between the states taken into ac-

count, as well as the densities of the SR pumping photons and low-energy pumping photons.

The following data are used as input: Original neutral Li gas density and temperature, pumping SR spectrum and intensity as a function of time, low-energy photon frequency and intensity as a function of time, and target dimensions. Approximations made in the calculation will be discussed next.

(1) Only those states are taken into account in the rate equations which are connected with the five largest oscillator strengths in the Li II ions, plus the ground state of the Li I atoms. This approximation is not inherent in the program and could be relaxed, but we do not believe that to be necessary for our present purposes. These six states are listed below, followed by the number with which the program labels those states:

- Li I $1s^2 2s$: No. 1 ,
- Li II $1s^2$: No. 2 ,
- Li II $1s 2s$: No. 3 ,
- Li II $1s 2p$: No. 4 ,
- Li II $1s 3p$: No. 5 ,
- Li II $1s 3d$: No. 6 .

The program also uses the labeling

- free electrons: No. 7 .

The oscillator strengths associated with No. $i \rightarrow$ No. j ($i, j = 1, 2, \dots, 6$) transitions are written as $f(i, j)$, and their values are²¹

$$\begin{aligned} f(2, 4) &= 0.457 , \\ f(3, 4) &= 0.213 , \\ f(4, 6) &= 0.714 , \\ f(2, 5) &= 0.111 , \\ f(3, 5) &= 0.256 . \end{aligned}$$

Denoting by g_i the statistical weight of state No. i , one has $g_i f(i, j) = g_j f(j, i)$.

(2) The program considers transitions caused by electron impact, photon impact, or by spontaneous radiative decay, as well as electron-impact ionization of the ground state of Li I. Atom- and ion-induced impact transitions are taken into account only approximately because, for cases of interest to us, their effect is minor.

(3) The simulation assumes a long narrow gas (plasma) volume, when all particle densities can be considered to be uniform across the height and width of the target, i.e., in the notation of Fig. 3, along d_x and d_y .

(4) Photon escape probabilities were calculated in two different ways. In the first approach, the effect on line shapes of photon propagation in the medium is taken into account only on the average. In the second, the line shape is calculated more accurately, but the photon escape probabilities are treated only approximately, by evaluating them for two classes of photons, "longitudinal" (i.e., those traveling parallel or almost parallel to the z axis) and

“transverse” (i.e., all other photons).

The program also evaluates the total energy absorbed by the sample from the incident synchrotron radiation, and the total energy of photons emitted in various directions. These numbers, of course, determine the energy efficiency of the laser.

Line shapes are calculated and possible plasma effects are included. One application of this computer simulation will be to find the best initial value parameters for the photons as well as the lasing medium, once the characteristics of the available experimental facility are specified.

B. Rate equations

We denote the density of state No. i , where $i=1, \dots, 6$, by N_i . The free-electron density will be written as N_7 . If the electron and photon densities are included in the rate constants, then the rate equations are linear in terms of the ionic densities N_i ($i=1, \dots, 6$). We introduce a six-dimensional vector \mathbf{N} whose components are defined to be N_i ($i=1, \dots, 6$). Then the rate equations take the form

$$\frac{d\mathbf{N}}{dt} = [\underline{A}(t) + \underline{D}(t) + \underline{B}(t)]\mathbf{N}(t). \quad (2)$$

Here t stands for the time, and the matrices \underline{A} , \underline{B} , and \underline{D} are defined as

$$A_{ij}(t) = N_7(t)K^{\text{el}}(j \rightarrow i) + [K^s(j \rightarrow i)]_{\epsilon_j > \epsilon_i}, \quad \text{if } i \neq j; \quad (2')$$

$$A_{ii}(t) = -N_7(t) \sum_j K^{\text{el}}(i \rightarrow j) - \sum_j [K^s(i \rightarrow j)]_{\epsilon_j < \epsilon_i};$$

and

$$D_{ij}(t) = \sum_q K^p(j \rightarrow i)p^q(i, j, t), \quad \text{if } i \neq j; \quad (2'')$$

$$D_{ii}(t) = - \sum_{q,j} K^p(i \rightarrow j)p^q(i, j, t),$$

where the various $K^{\text{el}}(j \rightarrow i)$ stand for the electron-impact transition rates between the various states considered (including excitation and ionization), the K^s and K^p denote the spontaneous radiative-decay rates and induced-photon-impact rates, respectively. The $p^q(i, j, t)$ denotes the photon density associated with the No. $i \rightleftharpoons$ No. j transition. The superscript q specifies the direction of photon propagation. In the following calculation we will sometimes be concerned with only two directions of propagation, longitudinal (to be defined later) and transverse (all directions which are not longitudinal). In that case, two values for q will be used, denoted by v and w , which stand for longitudinal and transverse, respectively.

The matrix \underline{B} represents the “driving elements” proportional to the synchrotron-radiation intensity. In the case of interest to us

$$\begin{aligned} B_{11} &= -(R_{1s} + R_{2s})I_0\Theta(\tau_0 - t), \\ B_{21} &= R_{2s}I_0\Theta(\tau_0 - t), \\ B_{31} &= R_{1s}I_0\Theta(\tau_0 - t), \end{aligned} \quad (2''')$$

where τ_0 is the duration of the synchrotron-radiation intensity I_0 , and the unit step function $\Theta(\tau_0 - t)$ is defined to be unity for $t \leq \tau_0$, and zero otherwise. We include the possibility that an additional driving element also exists, a beam of photons whose energy equals either the energy of Li II $1s2p = \text{Li II } 1s2s$ transitions, or the energy of Li I $1s^22p = \text{Li I } 1s^22s$ transitions. The R_{1s} and R_{2s} represent the ionization rates of neutral Li resulting in Li II $1s2s$ and Li II $1s^2$ ions, respectively, due to the incident SR.

The ionic densities are coupled to the photon densities through

$$\begin{aligned} \frac{d}{dt}p^q(i, j, t) &= G(i, j, t) + H(i, j, t)p^q(i, j, t) \\ &\quad - \mathbf{C}_q \cdot \nabla p^q(i, j, t), \end{aligned} \quad (3)$$

where

$$G(i, j, t) = N_j \chi(q) K^s(j \rightarrow i) \Theta(\epsilon_j - \epsilon_i), \quad (3')$$

$$H(i, j, t) = N_j K^p(j \rightarrow i) - N_i K^p(i \rightarrow j)$$

and, again, $p^q(i, j, t)$ is the density of photons traveling in the q direction, with energy ΔE_{ij} , and ΔE_{ij} is the transition energy in No. $i \rightleftharpoons$ No. j transitions. The \mathbf{C}_q is the photon velocity vector, i.e., its direction is q , while its magnitude is the speed of the photons under consideration in the medium (in our case, to a good approximation, this is the speed of light in a vacuum). The last term in Eq. (3) produces a space-dependent density distribution, determined by the boundary conditions. The $\chi(q)$ which represents an angular factor for the probability of spontaneous emission in the q direction, also depends on the geometry of the sample.

In order to simplify Eq. (2), the free-electron density can be written in the analytic form

$$N_7(t) = N_1^0 (1 - e^{-B_{11}t}), \quad (4)$$

which is correct if the free electrons are produced predominantly as a result of $\text{Li}(1s^22s) \rightarrow \text{Li}^+(1s2s) + e^-$ and $\text{Li}(1s^22s) \rightarrow \text{Li}^+(1s^2) + e^-$ ionization processes induced by the incident synchrotron radiation. In Eq. (4), N_1^0 is the initial neutral Li density, i.e., $N_1^0 = N_1(t=0)$.

To solve the coupled Eqs. (2) and (3), one can formally integrate Eq. (3) over time. Indicating explicitly, for the moment, the spatial dependence by an argument \mathbf{x} , one finds

$$\begin{aligned} p^q(i, j, t, \mathbf{x}) &= p^q(i, j, t=0, \mathbf{x} - \mathbf{C}_q t) \exp \left[\int_{t'=0}^{t'=t} H(i, j, t', \mathbf{x} - \mathbf{C}_q(t-t')) dt' \right] \\ &\quad + \left\{ \int_{t'=0}^{t'=t} G(i, j, t', \mathbf{x} - \mathbf{C}_q(t-t')) \left[\exp \left[\int_{t''=t'}^{t''=t} H(i, j, t'', \mathbf{x} - \mathbf{C}_q(t-t'')) dt'' \right] dt' \right\}. \end{aligned} \quad (5)$$

Specifying the initial condition for all $p^q(i, j, t, \mathbf{x})$ and all \mathbf{x} as

$$p^q(i, j, t=0, \mathbf{x})=0,$$

the first term on the right-hand side of Eq. (5) vanishes. Substituting this expression for p^q , Eq. (2) gives

$$\begin{aligned} \frac{d}{dt} N_i(t, \mathbf{x}) = & \sum_j [A_{ij}(t, \mathbf{x}) + B_{ij}(t, \mathbf{x})] N_j(t, \mathbf{x}) \\ & + \sum_j H(i, j, t, \mathbf{x}) \sum_q \int_{t'=0}^{t'=t} \chi(q) K^s(j \rightarrow i) \Theta(\epsilon_j - \epsilon_i) N_j(t', \mathbf{x} - \mathbf{C}_q(t-t')) \\ & \times \left[\exp \left[\int_{t''=t'}^{t''=t} H(i, j, t'', \mathbf{x} - \mathbf{C}_q(t-t'')) dt'' \right] \right] dt'. \end{aligned} \quad (6)$$

In this equation all quantities may vary in time as well as space. When coherent photon generation is to take place inside a long, narrow volume ($d_x, d_y \ll d_z$), and if the initial Li gas density is uniform and, also, the intensity variation of the pumping SR along the x and y axes can be neglected (see Fig. 3), then it may be justified to neglect the variation in space along the x and y axes, of all N , and $p^q(i, j)$. If, further, the long volume is subdivided into shorter sections along the z axis, and the length along z of each section is sufficiently small, then the spatial variation for N_i and for some of the $p^q(i, j)$ may be neglected altogether within each volume section. The time behavior of a pulse of photons with energy E_l can then be studied and reconstructed by following the history of its density, as a function of propagation direction, and time, within each volume section, while neglecting the spatial variation of all N_i and $p^q(i, j)$ within any one volume section. The permissible size of such volume sections depends on the geometry. For transverse pumping they may include the entire volume.

Whenever interactions between volume sections is negligible, the evolution of the system can be followed by studying the evolution of such volume sections by themselves. In particular, the gain can be calculated from the time evolution of one volume section.

C. Rate constants

The photoionization cross sections for removal from Li($1s^2 2s$) of a $1s$ or $2s$ electron, respectively, when the photon energy E is at the K -shell threshold energy $E_{x,K} = 66.3$ eV are

$$\begin{aligned} \sigma_{1s}^0 &= \sigma_{1s}(E = E_{x,K}) = 3.8 \times 10^{-18} \text{ cm}^2, \\ \sigma_{2s}^0 &= \sigma_{2s}(E = E_{x,K}) = 3.9 \times 10^{-20} \text{ cm}^2. \end{aligned}$$

When the photon energy is larger than $E_{x,K}$, but is sufficiently close to it, i.e., $(E - E_{x,K})/E_{x,K} \ll 1$, then the photon energy dependence of σ_{1s} and σ_{2s} can be approximated by the power law

$$\begin{aligned} \sigma_{1s}(E) &= \sigma_{1s}^0 \left[\frac{E}{E_{x,K}} \right]^{-\alpha_1}, \\ \sigma_{2s}(E) &= \sigma_{2s}^0 \left[\frac{E}{E_{x,K}} \right]^{-\alpha_2}, \end{aligned} \quad (7a)$$

where

$$\begin{aligned} \alpha_1 &= \frac{8}{3}, \\ \alpha_2 &= 1.4. \end{aligned} \quad (7b)$$

We will assume that the incident synchrotron radiation contains energies only within the range $(E_{x,L}, E_{x,M})$, where $E_{x,K} \leq E_{x,L}$, and $(E_{x,M} - E_{x,L})/E_{x,K} \ll 1$, and also assume that its intensity as a function of E is constant within this range. Then

$$R_{ls} = \sigma_{ls}^0 \frac{(E_{x,K})^{\alpha_l}}{1 - \alpha_l} [(E_{x,M})^{1-\alpha_l} - (E_{x,L})^{1-\alpha_l}]. \quad (8)$$

The average energy of the photoelectrons ejected during these two processes is

$$\bar{\epsilon} = (A_{1s} + A_{2s}) / (R_{1s} + R_{2s}),$$

where

$$A_{ls} = \int_{E_{x,L}}^{E_{x,M}} (E - E_{x,l}) \Theta(E - E_{x,l}) \sigma_{ls}(E) dE \quad (l=1,2) \quad (9)$$

and $E_{x,l}$ ($l=1,2$) is the threshold photon energy for K - and L -shell photoionization, respectively. In case of thermalization, the temperature of free (photo) electrons will be

$$T_{el} = \frac{1}{k} \frac{2}{3} \bar{\epsilon},$$

where, as usual, k is the Boltzmann constant.

Next we calculate the transition rates between various ionic states. The rate of spontaneous radiative decay is trivial, giving

$$K^s(j \rightarrow i) = \frac{2\alpha}{\hbar} \frac{(\Delta E_{ji})^2}{mc^2} f(j, i) \text{ sec}^{-1}, \quad (10)$$

where ΔE_{ji} is the transition energy, and α is the fine structure constant.

To calculate the transition rates caused by electron impact, we use for the electron-impact excitation cross section

$$\begin{aligned} \sigma_{i \rightarrow j}(\epsilon) &= 1.2\pi e^4 \frac{f(i, j)}{\Delta E_{ij}} \frac{1}{\epsilon} \ln \left[\left(\frac{Z^*}{Z^* + 1} + 1 \right) \frac{\epsilon}{\Delta E_{ij}} \right] \\ &\times [1 - \exp(-0.3\epsilon/\Delta E_{ij})]. \end{aligned} \quad (11)$$

The ϵ and Z^* denote the energy of the incident electron and the ionic charge ($Z^* = 0$ for neutrals), respectively.²²

When the free electrons have Maxwellian energy distribution, the rates can be calculated analytically:

$$K^{\text{el}}(i \rightarrow j) = \int_{\Delta E_{ij}}^{\infty} \sigma_{i \rightarrow j}(\epsilon) n(\epsilon) v(\epsilon) d\epsilon. \quad (12)$$

With

$$n(\epsilon) d\epsilon = \frac{2}{\pi^{1/2}} \frac{1}{(kT)^{3/2}} \epsilon^{1/2} e^{-\epsilon/kT} d\epsilon,$$

$$v(\epsilon) = c \left[\frac{2\epsilon}{mc^2} \right]^{1/2},$$

$$I(\Delta E, kT, Z^*) = \frac{kT}{\Delta E} \left\{ \left[\exp \left[\frac{-\Delta E}{kT} \right] \right] \ln \left[\frac{Z^*}{Z^*+1} + 1 \right] + E_1 \left[\frac{\Delta E}{kT} \right] \right\}$$

$$- \frac{kT}{\Delta E + 0.3kT} \left\{ \left[\exp \left[-\frac{\Delta E + 0.3kT}{kT} \right] \right] \ln \left[\frac{Z^*}{Z^*+1} + 1 \right] + E_1((\Delta E + 0.3kT)/kT) \right\}. \quad (13)$$

The transition rates due to ionic deexcitation caused by electron impact are

$$K^{\text{el}}(j \rightarrow i) = \frac{f(j,i)}{f(i,j)} \exp \left[\frac{\Delta E_{ij}}{kT} \right] K^{\text{el}}(i \rightarrow j), \quad (14)$$

as expected from detailed balance. For the electron-impact ionization cross section we use the similar formula to the one given by Lotz.²² Again, if the electron energy distribution is Maxwellian, the appropriate averaging over electron energies has to be taken.

The computation of photon-induced transition rates requires a knowledge of the appropriate line-shape function $b_{ij}(E)$. The integral of $b_{ij}(E)$ over E is defined to be unity, and the energy at which $b_{ij}(E)$ reaches its maximum is, by definition, ΔE_{ij} . The cross section for a line transition is

$$\sigma_{i \rightarrow j}(E) = 2\pi^2 \alpha f(i,j) b_{ij}(E) e^2 a_0, \quad (15)$$

where $b_{ij}(E)$ is the line-shape function in units of $a_0 e^2$, and a_0 is the Bohr radius, and the electron charge is denoted by e . The energy distribution of photons with energy ΔE_{ij} is assumed to be the same as the line-shape function which gives

$$K^{\text{p}}(i \rightarrow j) = 2\pi^2 \alpha c f(i,j) e^2 a_0 \int_{-\infty}^{+\infty} [b_{ij}(E)]^2 dE. \quad (16)$$

In the case of Doppler broadening,

$$b_{ij}(E) = \frac{1}{\pi^{1/2} \Gamma_{ij}} \exp \left[- \left[\frac{E - \Delta E_{ij}}{\Gamma_{ij}} \right]^2 \right],$$

and

$$\int_{-\infty}^{+\infty} [b_{ij}(E)]^2 dE = \frac{1}{(2\pi)^{1/2}} \frac{1}{\Gamma_{ij}},$$

and

$$E_1(x) = \int_x^{\infty} \frac{e^{-t}}{t} dt,$$

one has

$$K^{\text{el}}(i \rightarrow j) = 2c\pi^{1/2} 1.2e^4 f(i,j) \left[\frac{2}{mc^2} \right]^{1/2} (kT)^{-3/2}$$

$$\times I(\Delta E_{ij}, kT, Z^*),$$

where

so that

$$K^{\text{p}}(i \rightarrow j) = 2^{1/2} \pi^{3/2} \alpha c e^2 a_0 f(i,j) / \Gamma_{ij}. \quad (17)$$

In the case of Lorentz broadening, on the other hand, one has

$$b_{ij}(E) = \frac{\gamma_{ij}}{\pi} [(E - \Delta E_{ij})^2 + \gamma_{ij}^2]^{-1}$$

and

$$\int_{-\infty}^{+\infty} [b_{ij}(E)]^2 dE = \frac{1}{2\pi\gamma_{ij}},$$

so that

$$K^{\text{p}}(i \rightarrow j) = \pi \alpha c e^2 a_0 f(i,j) / \gamma_{ij}. \quad (18)$$

IV. PHOTON ESCAPE PROBABILITIES AND LINE SHAPES

Photon escape from the lasing volume was calculated in two different ways.

(1) Within the volume section under consideration, the spatial variation of ionic densities is neglected, i.e., we set

$$N_i(t, \mathbf{x}) \approx N_i(t) \Theta(\mathbf{d} - \mathbf{x}), \quad i = 1, 2, \dots, 6$$

where we define $\Theta(\mathbf{d} - \mathbf{x})$ to be that function whose value is unity when \mathbf{x} is located within the volume segment under consideration, and zero otherwise. That segment has a shape shown in Fig. 3. Note, that for this segment the length d will be less than the length of the lasing volume, except if the volume section under consideration encompasses the entire lasing volume. Then one can write Eq. (6) as

$$\frac{d}{dt} N_i(t) = \sum_j [A_{ij}(t) + B_{ij}(t)] N_j(t) + \sum_j H(i,j,t) \sum_q \left[\Theta(\mathbf{L}_q - \mathbf{C}_q t) \int_{t'=0}^{t'=t} + \Theta(\mathbf{C}_q t - \mathbf{L}_q) \int_{t'=t-L_q/c}^{t'=t} \right]$$

$$\times \chi(q) K^s(j \rightarrow i) N_j(t') \exp \left[\int_{t''=t'}^{t''=t} H(i,j,t'') dt'' \right] dt'.$$

Here the first (second) term in the large parentheses refers to the case when a photon traveling in the q direction traverses the volume section (traveling a distance L_q inside the section) during a time interval which is larger (smaller) than t .

(2) All photons are divided into two classes: (a) To the first class belong longitudinal photons, i.e., those photons which travel either parallel to the z axis or else within a narrow angle α measured from the z axis. Assuming $d_y \leq d_x$, choose $\alpha = d_y/d_x$. (b) The second class encompasses photons traveling in all other directions.

To include the effect of photon escape from the sample, Eq. (3) is used directly, but the last term in it is replaced by an "effective photon escape probability": $p^q(i,j,t)c/L_q$, where c is the speed of light in a vacuum and L_q represents the linear dimension of the volume along the q direction. The L_q is chosen to be d_z and d_y for photons belonging to classes (a) and (b), respectively.

In case (a) one does not have to perform an integration over photon propagation direction angles, while in case (b) such an integration is required. (For details, see Appendix.)

V. RESULTS

Calculations were performed for lasing volumes for which $d_z = 1$ cm and $d_x = d_y = 10^{-3}$ and 10^{-4} cm. The time evolution of the lasing medium and that of the photons in the medium was followed for 4×10^{-11} sec after commencement of the sample by synchrotron photons.

At the initial moment the neutral Li I $1s^2 2s$ atoms inside the volume are assumed to either have number density 10^{19} cm $^{-3}$ and a temperature of 0.15 eV = 1791 K, or else number density 3×10^{18} cm $^{-3}$ and a temperature of 0.13 eV = 1600 K. These temperatures are so chosen that the Li atomic species will be able to achieve the required density at the chosen temperature and, in addition, so that the Li $_2$ molecular species density is relatively low. Based on this observation, the presence of Li $_2$ molecules are ignored in the calculation.

The energy of the pumping synchrotron-radiation photons lies in the interval between $E_{x,L} = E_{x,K} = 66.3$ eV, and $E_{x,M}$. The photon intensity within this interval is assumed to be uniform. We chose $E_{x,M} - E_{x,L} = 2$ or 3 eV.

As a function of time, the synchrotron-radiation intensity is assumed to be step functionlike: at the initial moment the intensity jumps to its peak value of $I_0/(E_{x,M} - E_{x,L})$ and persists at that value for a time $\tau_0 = 2 \times 10^{-11}$ sec. That peak value is chosen to be 10^{26} cm $^{-2}$ sec $^{-1}$ eV $^{-1}$, or 3×10^{26} cm $^{-2}$ sec $^{-1}$ eV $^{-1}$.

The sample is irradiated with low-energy photons of energy 1.30 eV, which will induce Li II $1s2s \rightleftharpoons$ Li II $1s2p$ transitions. The intensity of these photons jumps to I_{0L} at the initial moment and persists at that value for a time $\tau_0 = 2 \times 10^{-11}$ sec. The value of I_{0L} is chosen to be 10^{26} cm $^{-2}$ sec $^{-1}$.

During times of interest to us, no significant equalization of ionic and electronic temperatures occur for the conditions specified. On the other hand, electrons tend to thermalize substantially. In the calculations carried out, complete thermalization is assumed, which is a conserva-

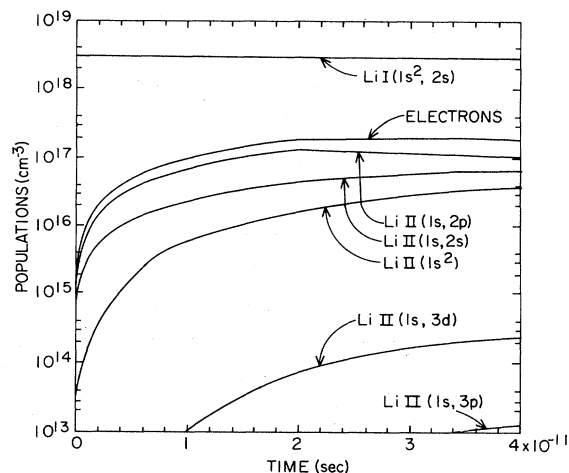


FIG. 5. Evolution of atomic, ionic, and electronic densities for initial Li I $1s^2 2s$ atomic density 3×10^{18} cm $^{-3}$, ion temperature 0.13 eV, $E_{x,M} - E_{x,L} = 3$ eV, and $d_x = d_y = 10^{-3}$ cm.

tive assumption, since it tends to depress the calculated gain.

Pumping is assumed to be exactly transverse, so that density variations within the lasing volume can be neglected. The results can also be used directly to evaluate the behavior of the system under other methods of pumping. For a wide range of parameters the gain is expected to be close to the one evaluated here for transverse pumping and that, in turn, allows a direct calculation of the flux of coherent photons produced by the laser.

Figure 5 shows the time evolution of ionic species within the lasing volume, for various chosen parameter values. The time evolution of longitudinal photons within the lasing volume for the same values of the chosen parameters is displayed in Fig. 6, while Fig. 7 shows the time evolution of the laser gain.

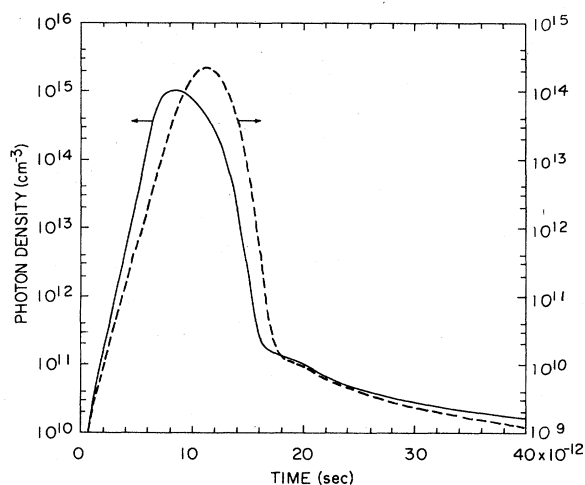


FIG. 6. Longitudinal photon density for parameter values as in Fig. 5 (solid line) and for initial Li I $1s^2 2s$ atomic density 10^{19} cm $^{-3}$, ion temperature 0.15 eV, $E_{x,M} - E_{x,L} = 2$ eV, and $d_x = d_y = 10^{-4}$ cm (dashed line).

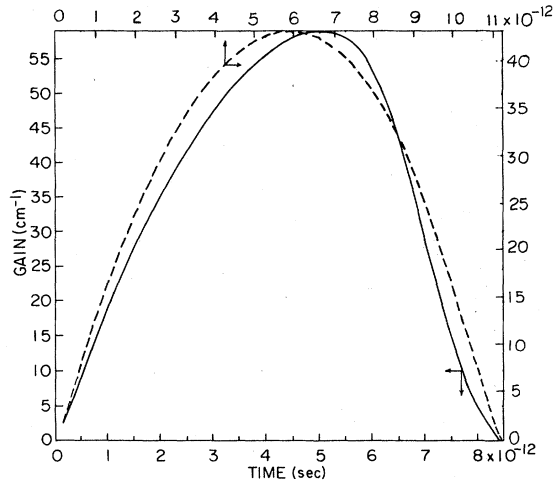


FIG. 7. Laser gain for parameter values as in Fig. 5 (solid line) and for parameter values as in Fig. 6 (dashed line).

APPENDIX

The following notation will be used in this appendix. The distance of a photon-emitting ion or atom from a chosen sample surface will be denoted by x . The number density of the relevant ions in the sample is ρ (and has the dimension cm^{-3}). For discrete lines the cross section is given by Eq. (15).

1. Narrow-angle propagation

In this case x is chosen to be the distance of the photon-emitting ion from the far end of the sample. The escape probability is, in general,

$$P_{ij}(x, \hbar\omega) = \exp[-\sigma(\hbar\omega)\rho l] = \exp[-C_{ij}b(\hbar\omega)x],$$

where l denotes the distance traveled by the emitted photon inside the sample. In the present case, $l=x$. The C_{ij} is defined as

$$C_{ij} = 2\pi^2 \alpha f(i, j) \rho e^2 a_0,$$

and has the dimension erg cm^{-1} .

Averaging $P_{ij}(x, \hbar\omega)$ over the line shape, one obtains

$$\begin{aligned} P_{ij}(x) &= \int_{-\infty}^{+\infty} b(\hbar\omega) P_{ij}(x, \hbar\omega) d(\hbar\omega) \\ &= \int_{-\infty}^{+\infty} b(\hbar\omega) \exp[-C_{ij}b(\hbar\omega)x] d(\hbar\omega). \end{aligned}$$

Further averaging of $P_{ij}(x)$ over a distance L leads to

$$\begin{aligned} P_{ij} &= \frac{1}{L} \int_0^L P_{ij}(x) dx \\ &= \frac{1}{LC_{ij}} \int_{-\infty}^{+\infty} \{1 - \exp[-C_{ij}b(\hbar\omega)L]\} d(\hbar\omega). \end{aligned}$$

2. Wide-angle propagation

Now x is defined as the distance between the location Q of the photon-emitting ion, from the nearest sidewall of

the sample, i.e., as the distance between Q and the normal projection Q' of Q onto that sidewall. Denote by Θ the angle between the direction of propagation of the emitted photon and the line connecting Q and Q' . Then $l = x / \cos\Theta$. In this case, defining $z = (\cos\Theta)^{-1}$,

$$P_{ij}(x, \hbar\omega, \Theta) = \exp[-\sigma(\hbar\omega)\rho l] = \exp[-C_{ij}b(\hbar\omega)xz].$$

An integration over Θ yields

$$\begin{aligned} P_{ij}(x, \hbar\omega) &= \int_0^{\pi/2} P_{ij}(x, \hbar\omega, \Theta) \sin\Theta d\Theta \\ &= \exp[-C_{ij}b(\hbar\omega)x] \\ &\quad - C_{ij}b(\hbar\omega)x E_1[C_{ij}b(\hbar\omega)x]. \end{aligned}$$

To perform an averaging over distance l of $P_{ij}(x, \hbar\omega, \Theta)$, we first integrate over x and then over z :

$$\begin{aligned} P_{ij}(\hbar\omega) &= \frac{1}{L} \int_0^L \int_1^\infty \exp[-C_{ij}b(\hbar\omega)xz] \frac{1}{z^2} dz dx \\ &= \frac{1}{2y} [1 - e^{-y} + ye^{-y} - y^2 E_1(y)], \end{aligned}$$

where

$$y = LC_{ij}b(\hbar\omega).$$

Since for $y \rightarrow 0$ one has $yE_1 \rightarrow 0$, the $P_{ij} \rightarrow 0$ in this limit.

Finally, additional averaging over the line shape gives

$$\begin{aligned} P_{ij} &= \int_{-\infty}^{+\infty} P_{ij}(\hbar\omega) b(\hbar\omega) d(\hbar\omega) \\ &= \frac{1}{2LC_{ij}} \int_{-\infty}^{+\infty} [1 + (y-1)e^{-y} - y^2 E_1(y)] d(\hbar\omega). \end{aligned}$$

When the line-shape function has a Lorentzian profile, we distinguish the corresponding P_{ij} with an additional subscript "Lor." In cases (a) and (b) a superscript v and w will be affixed, respectively. One finds

$$P_{ij, \text{Lor}}^v = -\frac{2}{u} \int_0^{+\infty} \left[1 - \exp\left[-\frac{u}{\pi} \frac{1}{s^2+1}\right] \right] ds, \quad (\text{A1a})$$

where $s = \hbar\omega/\gamma$ was used, and $u = C_{ij}L/\gamma$,

$$\begin{aligned} P_{ij, \text{Lor}}^w &= \frac{1}{u} \int_0^{+\infty} \left[1 - \exp\left[-\frac{u}{\pi} \frac{1}{s^2+1}\right] \right. \\ &\quad \left. + \frac{u}{\pi} \frac{1}{s^2+1} \exp\left[-\frac{u}{\pi} \frac{1}{s^2+1}\right] \right. \\ &\quad \left. - \frac{u^2}{\pi^2} \frac{1}{(s^2+1)^2} E_1\left[\frac{u}{\pi} \frac{1}{s^2+1}\right] \right] ds. \end{aligned} \quad (\text{A1b})$$

The expressions given in Eqs. (A1a) and (A1b) are used in Eq. (3). All widths (i.e., Doppler, electron impact, as well as Stark) are then lumped together, yielding a single effective Lorentzian width Γ . Expressions (A1a) and (A1b) are functions of u only, for which accurate polynomial approximations were obtained, and those appear in the computation.

- *Present address: National Synchrotron Light Source, Brookhaven National Laboratory, Upton, NY 11973.
- ¹Paul L. Csonka, University of Oregon Institute of Theoretical Science Report No. NT-055/74, 1974 (unpublished); *Phys. Rev. A* **13**, 405 (1976).
- ²Paul L. Csonka, Stanford Synchrotron Radiation Laboratory Report No. SSRL-77/03, 1977 (unpublished).
- ³M. A. Duguay and P. M. Rentzepis, *Appl. Phys. Lett.* **10**, 350 (1967).
- ⁴S. A. Mani, H. A. Hyman, and J. D. Daugherty, *J. Appl. Phys.* **47**, 3099 (1976); H. A. Hyman and S. A. Mani, *Opt. Commun.* **20**, 209 (1976); S. E. Harris, *Opt. Lett.* **5**, 1 (1980); R. G. Caro, J. C. Wang, R. W. Falcone, J. F. Young, and S. E. Harris, *Appl. Phys. Lett.* **42** (1), 9 (1983); R. G. Caro, J. C. Wang, J. F. Young, and S. E. Harris, *Phys. Rev. A* **30**, 1407 (1984).
- ⁵For example, at Stanford the SPEAR ring magnet lattice has been rearranged during 1984 to reduce photon emittance.
- ⁶Three of them are now simultaneously in operation at the SPEAR ring.
- ⁷G. Brown, K. Halbach, J. Harris, and H. Winick, *Nucl. Instrum. Methods* **208**, 65 (1983).
- ⁸R. Tatchyn, in *Proceedings of the SPIE, Conference on Soft X-ray Science, Brookhaven, N.Y.* (in press).
- ⁹Eberhard Spiller, Armin Segmuller, and Rolf-Peter Haelbich, in *Conference on Ultrasoft X-ray Microscopy* (New York Academy of Sciences, New York, 1979).
- ¹⁰James H. Underwood and Troy W. Barbee, Jr., *Nature* (London) **294**, 429 (1981).
- ¹¹Roman O. Tatchyn and Ingolf Lindau, *Nucl. Instrum. Methods* **172**, 287 (1980).
- ¹²Roman O. Tatchyn, Paul L. Csonka, and Ingolf Lindau, *J. Opt. Soc. Am.* **72**, 1630 (1982).
- ¹³Paul L. Csonka, *J. Appl. Phys.* **52**, 2692 (1981).
- ¹⁴E. Kallne, *Nucl. Instrum. Methods* **195**, 105 (1982).
- ¹⁵Roman O. Tatchyn, Paul L. Csonka, and E. Ingolf Lindau, *IEEE J. Quantum Electron.* **QE-19**, 1821 (1983).
- ¹⁶Paul L. Csonka, in *Wiggler Magnets*, edited by H. Winich and J. Knight (unpublished); Stanford Synchrotron Radiation Laboratory, Report No. SSRL 77/05, 1977 (unpublished), and Stanford Synchrotron Radiation Laboratory, Report No. SSRL 79/04, 1979 (unpublished); *Part. Accel.* **8**, 225 (1978); **11**, 45 (1980).
- ¹⁷Avi Gover, Paul L. Csonka, and D. Deacon, in *Proceedings of the New Rings Workshop, Stanford, Stanford Synchrotron Radiation Laboratory, Report No. SSRL 83/02, 1983* (unpublished).
- ¹⁸Paul L. Csonka, University of Oregon Institute of Theoretical Science Report No. NT-065/77, 1977 (unpublished).
- ¹⁹Paul L. Csonka, *Nucl. Instrum. Methods* **137**, 131 (1976).
- ²⁰Paul L. Csonka, *Nucl. Instrum. Methods* **131**, 267 (1975).
- ²¹W. L. Wiese, M. W. Smith, and B. M. Glennon, *Atomic Transition Probabilities, Vol. I*, Natl. Bur. Stand. (U.S. GPO, Washington, D.C., 1966).
- ²²This equation is similar to that given in Wolfgang Lotz, *As-trophys. J. Suppl. Ser.* **14**, 207 (1967).